NAVAL POSTGRADUATE SCHOOL
Monterey, California

THESIS

SHALLOW WATER ACOUSTIC VARIABILITY AND
INFLUENCES ON AUTOCORRELATION MATCHING
LOCALIZATION ALGORITHMS

Arthur F. Bettega Correa

December 1998

Thesis Advisor: Kevin B. Smith
Second Reader: Mitchell Shipley

Approved for public release; distribution is unlimited.

REPORT DOCUMENTATION PAGE

Form Approved
OMB No. 0704-0188

Public reporting burden for this collection of information is estimated to average 1 hour per response, including the time for reviewing instruction, searching existing data sources, gathering and maintaining the data needed, and completing and reviewing the collection of information. Send comments regarding this burden estimate or any other aspect of this collection of information, including suggestions for reducing this burden, to Washington headquarters Services, Directorate for Information Operations and Reports, 1215 Jefferson Davis Highway, Suite 1204, Arlington, VA 22202-4302, and to the Office of Management and Budget, Paperwork Reduction Project (0704-0188) Washington DC 20503.

1. AGENCY USE ONLY *(Leave blank)*	2. REPORT DATE December 1998	3. REPORT TYPE AND DATES COVERED Master's Thesis

4. TITLE AND SUBTITLE Shallow Water Acoustic Variability and Influences on Autocorrelation Matching Localization Algorithms	5. FUNDING NUMBERS
6. AUTHOR(S) Arthur F. Bettega Correa	

7. PERFORMING ORGANIZATION NAME(S) AND ADDRESS(ES) Naval Postgraduate School Monterey, CA 93943-5000	8. PERFORMING ORGANIZATION REPORT NUMBER

9. SPONSORING / MONITORING AGENCY NAME(S) AND ADDRESS(ES)	10. SPONSORING / MONITORING AGENCY REPORT NUMBER

11. SUPPLEMENTARY NOTES

The views expressed in this thesis are those of the author and do not reflect the official policy or position of the Department of Defense or the U.S. Government.

12a. DISTRIBUTION / AVAILABILITY STATEMENT Approved for public release; distribution is unlimited.	12b. DISTRIBUTION CODE

ABSTRACT *(maximum 200 words)*

In this work, several algorithms based on higher-order moment (autocorrelation) matching of single hydrophone element data have been developed and tested on real transient data sets. Of particular interest is the success and robustness of the Frequency-Domain Autocorrelation Matching (FACM) algorithms in the presence of environmental mismatch, signal mismatch, and noise, for different signals in an unknown environment. Recently acquired data was analyzed for signal variability in terms of spatial coherence of phones, beams, and modal structure. The ability to localize using these higher-order moment matching algorithms was compared to the spatial structure of the signal, the placement of the receiving elements, and the signal variability.

This work suggests that the FACM algorithms are strongly dependent on the source-receiver relative positions, and on the uniqueness of the signal vertical structure. It is also shown that their performance increases with the number of multipath arrivals and, therefore, with the range. More importantly, the localization results obtained with raw linear frequency modulated (LFM) signals seemed to be as useful as the ones obtained from matched-filtered data.

14. SUBJECT TERMS Transient Localization, Autocorrelation Matching, Plane-Wave Beamforming, Modal Decomposition .			14. NUMBER OF PAGES 66
			16. PRICE CODE

17. SECURITY CLASSIFICATION OF REPORT Unclassified	18. SECURITY CLASSIFICATION OF THIS PAGE Unclassified	19. SECURITY CLASSIFI- CATION OF ABSTRACT Unclassified	20. LIMITATION OF ABSTRACT UL

SHALLOW WATER ACOUSTIC VARIABILITY AND INFLUENCES ON AUTOCORRELATION MATCHING LOCALIZATION ALGORITHMS

Arthur F. Bettega Correa
Lieutenant, Brazilian Navy
B. S., Escola Naval, 1986

Submitted in partial fulfillment of the
requirements for the degree of

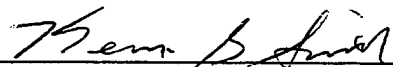## MASTER OF SCIENCE IN ENGINEERING ACOUSTICS

from the

NAVAL POSTGRADUATE SCHOOL
December 1998

Author: _____
Arthur F. Bettega Correa

Approved by: _____
Kevin B. Smith, Thesis Advisor

_____
Mitchell Shipley, Second Reader

_____
Kevin B. Smith, Chairman
Engineering Acoustics Academic Group

ABSTRACT

In this work, several algorithms based on higher-order moment (autocorrelation) matching of single hydrophone element data have been developed and tested on real transient data sets. Of particular interest is the success and robustness of the Frequency-domain Autocorrelation Matching (FACM) algorithms in the presence of environmental mismatch, signal mismatch, and noise, for different signals in an unknown environment. Recently acquired data was analyzed for signal variability in terms of spatial coherence of phones, beams, and modal structure. The ability to localize using these higher-order moment matching algorithms was compared to the spatial structure of the signal, the placement of the receiving elements, and the signal variability.

This work suggests that the FACM algorithms are strongly dependent on the source-receiver relative positions, and on the uniqueness of the signal vertical structure. It is also shown that their performance increases with the number of multipath arrivals and, therefore, with the range. More importantly, the localization results obtained with raw linear frequency modulated (LFM) signals seemed to be as useful as the ones obtained from matched-filtered data.

TABLE OF CONTENTS

LIST OF FIGURES

I. INTRODUCTION

In the past, passive sonar systems were only able to provide bearing information, and the estimation of source range relied on analytical, over-simplified techniques. Starting in the mid-60's, however, with relatively advanced computational resources, the received signals have been processed in order to also provide information about the distance to the source. Today, one of the most used and successful research techniques is matched-field processing (MFP) where a comparison is made between the parameters of the received signal and those of signals generated by a synthetic source virtually positioned at each point in the search grid. A match is obtained when the correlation of the synthetic and the true signals are at a maximum.

Transient signals are especially important for naval purposes, since they can represent several instances of a ship's routine, such as firing a torpedo, opening of hatches, starting of pumps, etc. Therefore, the Transient Localization Project at the Naval Postgraduate School has been studying, since 1993, several algorithms for localizing transient sources based on methods similar to MFP.

In 1995, three distinct schemes were studied: (a) the fully coherent localization, which was considered impractical as it required an extremely precise (and unavailable) propagation model, along with accurate environmental descriptions; (b) the semi-coherent localization, which correlated only the slower varying amplitude terms of the signal, trying to surpass the limitations of method (a); and (c) the autocorrelation matching, which

compared the autocorrelations of the received and modeled signals using a simple Bartlett technique. The NPS results showed that method (b) was not successful in localizing the signals of naval interest, and method (c), while not perfectly consistent, was the most useful technique. According to Miller et al. (1996), autocorrelation matching has an advantage over the other methods, since its processing allows the notching of the noise energy and the possibility of a multi-transient gain.

A. THE NUWC-TSP EXPERIMENT

The transient signal processing (TSP) experiment was a field study sponsored by NUWC, and conducted both by NUWC and C&M Tech., Inc. on 28-31 July 1997. Its purpose was to provide data to study the influence of a highly variable shallow water environment on acoustic propagation, and the effectiveness of localization algorithms.

The study area is shown in Figure 1.1 and as it is influenced by oceanographic and geological processes related to the shelfbreak, it provides a complex coastal environment for sound propagation. The continental shelf water is cold, and it presents large variations with location and season. The slope water, on the other hand, is warmer and influenced by the Gulf Stream.(Miller, C. W., 1998)
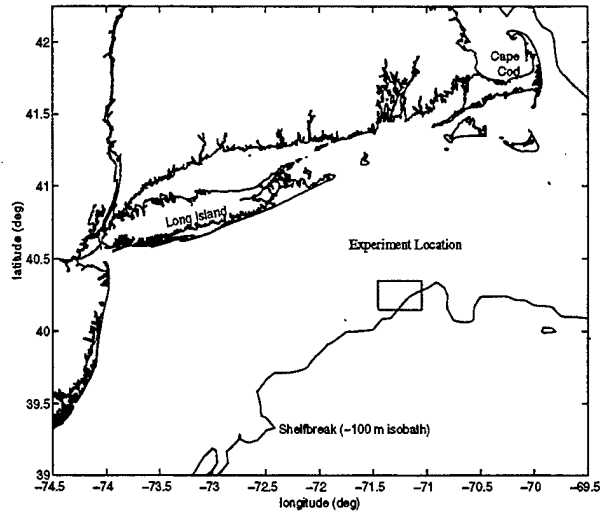
Figure 1.1. The NUWC-TSP Experiment Geographic Location.

Synthetic signals were generated and transmitted in a variety of scenarios which were differentiated by the source depth, source-receiver range, and bearing. Two projectors (ITC-104 and HX-188), a 32-element vertical-line hydrophone array (VLA), and data-recording equipment constituted the main assets of the experiment. The VLA configuration is depicted in Figure 1.2, and the experiment configuration for one of the scenarios is shown in Figure 1.3.

3
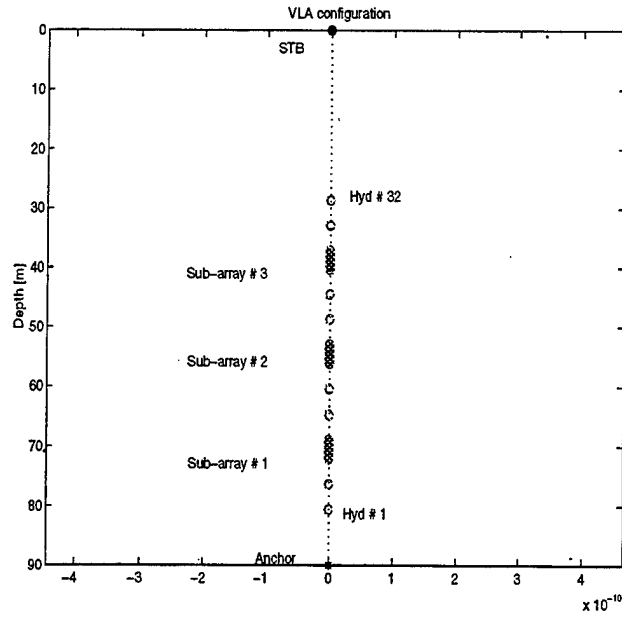
Figure 1.2. The VLA Configuration.
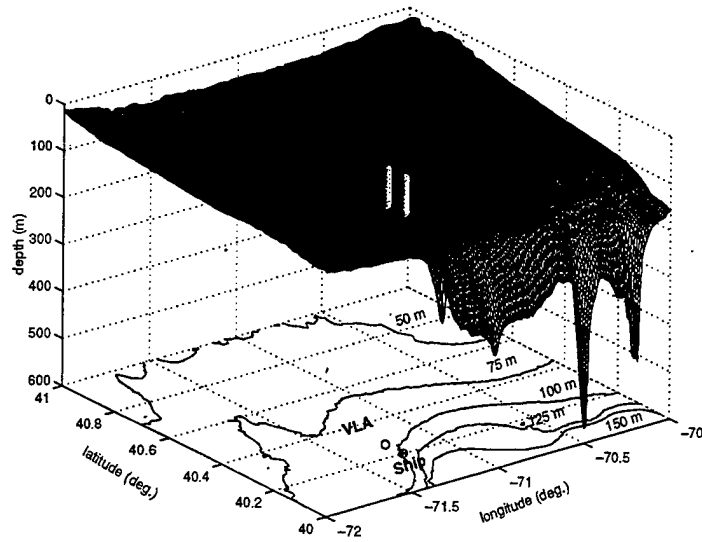
Figure 1.3. The NUWC-TSP Experiment Configuration.

4

It is important to note that hydrophones 17 and 18 were non-operative throughout the experiment. In this work, we were only interested in the linear frequency modulated (LFM), short duration (100 ms) signals - the transmitted chirp and a sample of a received burst can be seen in Figure 1.4. Their frequency spectra are observed in Figure 1.5.

The processed data corresponded to three particular cases: scenario 9 (source located at 4650 m range, 45.7 m depth), scenario 11 (source at 460 m range, 45.7 m depth), and scenario 16 (source at 2194 m range, 27.4 m depth). The information on source location was provided by NUWC, based on ship's log and GPS data. While some uncertainties are present in this information, inherited from the processes used to gather it, we assumed it as our reference. The recorded tapes also contain array tilt information, which was neglected in this work for simplicity.
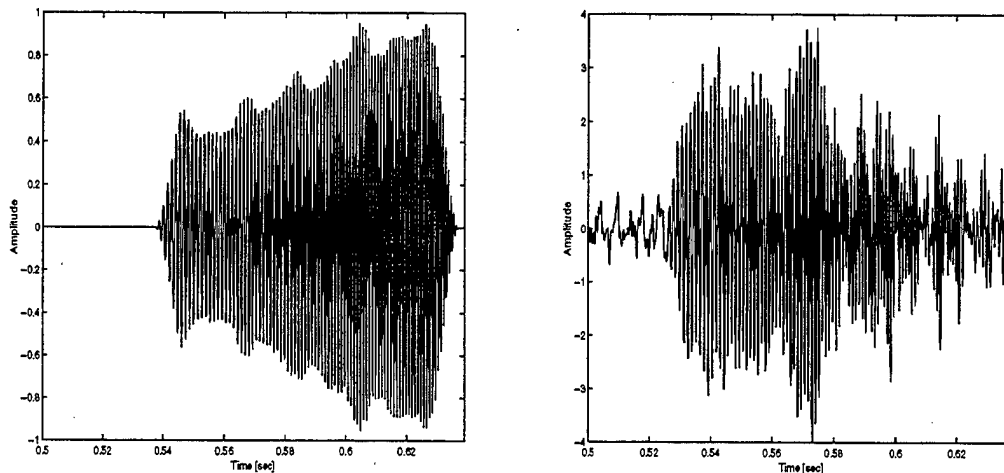
Figure 1.4. The Transmitted LFM Burst (Left) and the Received Signal at VLA (Right) in the Time-Domain. Note That the Axis Are Different on Each Plot.
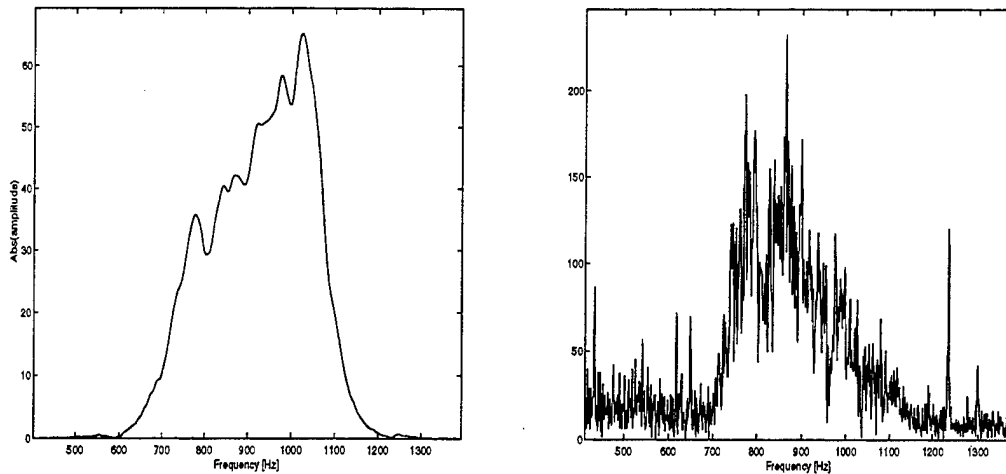
Figure 1.5. Frequency Spectra of Transmitted Chirp (Left) and Received Burst (Right).

In order to support the analysis of the experimental data, six conductivity-temperature-depth (CTD) casts were made. Two of them did not present useful data and were disregarded. The other four provided the sound speed profiles (SSP) shown in Figure 1.6, which also displays the date and time (Zulu) they were taken. For processing, however, we used only SVj97_08 (applied to scenario 9), and SVj97_12 (applied to scenarios 11 and 16), because they were gathered at times closer to those of the studied runs. Still, it is important to note the large variations, particularly near the lower part of the thermocline between 20-35 m. The associated pycnocline supports the propagation of nonlinear soliton waves which travel from the edge of the slope onto the shelf. Such oceanographic features can create localized regions of high sound speed contrast as strong as 25 m/s over a 100 m horizontal range in the direction of the soliton propagation (Chiu et al., 1997).
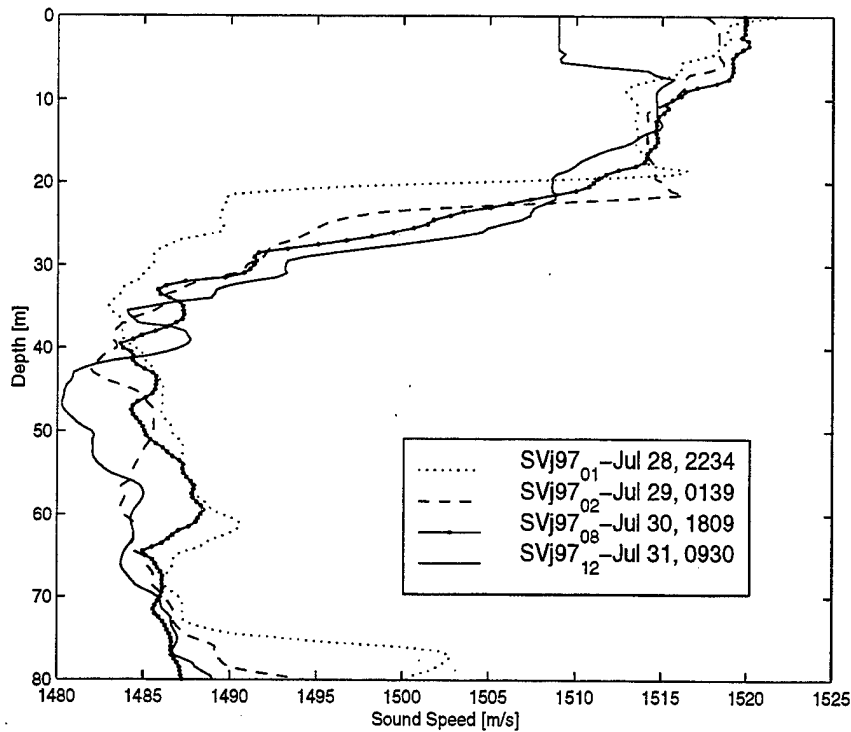
Figure 1.6. Sound Speed Profiles (SSP's) Collected During Experiment.

B. THESIS OBJECTIVE APPROACH AND OUTLINE

The objective of this thesis is to examine the influence of shallow water acoustic variability on frequency-domain autocorrelation matching (FACM) localization. In order to perform such analysis, we processed the acoustic VLA data, identified the LFM bursts, and high-pass filtered them to reduce the array strum influence (cut-off at 50 Hz). The resulting bursts, as well as the replicas generated by the MMPE propagation model, were applied to a Bartlett-type processor based on matching broadband signal autocorrelation

7

localization algorithm). The acoustics variability study followed with the plane-wave beamforming, modal amplitude structure, and spatial coherence analyses.

The remainder of this thesis consists of five chapters. Chapter II describes the Monterey-Miami Parabolic Equation (MMPE) propagation model. Chapter III discusses the Frequency-domain Autocorrelation Matching (FACM) localization algorithm. Chapter IV describes the techniques used to evaluate the environmental influences and process the signals. Chapter V presents the localization results. Chapter VI concludes this study with a summary of findings and recommendations for future work.

II. THE MONTEREY-MIAMI PARABOLIC EQUATION PROPAGATION MODEL

The Monterey-Miami Parabolic equation (MMPE) acoustic propagation model (Smith, K., 1996) was used to generate the replicas which simulated the received signals from a synthetic source on the gridpoints of a 2-D search space (depth x range). It allowed us to predict the arrival structure at the VLA due to a transient-like, broadband, point source. In this chapter, we introduce the general theory behind the parabolic equation model, as well as the method used for its implementation - the Split-Step Fourier (SSF) method (Hardin and Tappert, 1973).

The parabolic equation method for computing underwater acoustic propagation was introduced by Tappert (1977). To begin the parabolic approximation development, consider the representation of the time-harmonic acoustic field in cylindrical coordinates

$$P(r, z, \phi, f, t) = p_f(r, z, \phi)e^{-i2\pi ft} . \tag{1}$$

As the model is based on an approximation to the Helmholtz wave equation, substituting Eq. 1 into the latter in cylindrical coordinates leads to (Jensen et al., 1994)

$$\frac{1}{r}\frac{\partial}{\partial r}\left(r\frac{\partial p_f}{\partial r}\right) + \frac{1}{r^2}\frac{\partial^2 p_f}{\partial \phi^2} + \frac{\partial^2 p_f}{\partial z^2} + k_o^2 n^2 p_f = -4\pi P_o \delta(\vec{r} - \vec{r_s}) , \tag{2}$$

9

where $n(r, z, \phi) = \dfrac{c_o}{c(r, z, \phi)}$ is the acoustic index of refraction, c_o is the reference sound speed, $c(r, z, \phi)$ is the acoustic sound speed, and $k_o = \dfrac{\omega}{c_o}$ is the reference wave number.

In this derivation, however, we neglected density variations, which could be incorporated into a new index of refraction without any loss of generality. Note also that the environmental characteristics are within $c(r, z, \phi)$, and the reference pressure level P_o is defined as the pressure amplitude at a distance $R_o = 1$.

By assuming the ocean acts as a waveguide with a cylindrical coordinate system, acoustic energy is primarily propagated outward from a source in the horizontal direction. The pressure field, therefore, can be approximated by

$$p_f(r, z, \phi) = \psi_f(r, z, \phi) H_o^{(1)}(k_o r), \tag{3}$$

where the slowly varying envelope $\psi_f(r, z, \phi)$ modulates the outgoing zero-th order Hankel function of first kind $H_o^{(1)}(k_o r)$.

In the far field $(k_o r \gg 1)$, we can approximate the Hankel function by the first term of its asymptotic expansion (Gradshteyn and Ryzhik, 1994),

$$H_o^{(1)}(k_o r) = \sqrt{\frac{2}{i \pi k_o r}} e^{i k_o r}, \tag{4}$$

and Eq. 3 becomes

$$p_f(r, z, \phi) = P_o \sqrt{\frac{R_o}{r}} \psi_f(r, z, \phi). \tag{5}$$

Note that Eq. 5 is normalized such that at $r = R_o$, $|\psi| = 1$ and $|p_f| = P_o$. It expresses

the relationship between the PE field function $\psi(r, z, \phi)$ and the acoustic pressure

$p_f(r, z, \phi)$. By substituting it into Eq. 2 and dropping the source term on the right hand

side, we obtain

$$\frac{\partial^2 \psi}{\partial r^2} + i2k_o\frac{\partial \psi}{\partial r} + \frac{1}{r^2}\frac{\partial^2 \psi}{\partial \phi^2} + \frac{\partial^2 \psi}{\partial z^2} + \left[k_o^2(n^2 - 1) + \frac{1}{4r^2}\right]\psi = 0. \tag{6}$$

If we neglect the azimuthal coupling and the far field terms, Eq. 6 can be written as

$$\frac{i}{k_o}\frac{\partial \psi}{\partial r} = (T_{op} + U_{op})\psi, \tag{7}$$

where

$$T_{op} \equiv -\frac{1}{2k_o}\left(\frac{\partial^2}{\partial z^2}\right) \tag{8}$$

and

$$U_{op} \equiv -\frac{1}{2}(n^2 - 1). \tag{9}$$

Note that this is only valid for $\frac{\partial^2 \psi}{\partial \phi^2} \ll \psi$, once we used the uncoupled azimuth

approximation.

11

Eq. 7 is known as the standard parabolic equation (SPE), and the accurate solutions are limited to a half beam width of $10°$ to $20°$ for the propagation angle. However, in order to extend this limit to $40° \sim 70°$, a higher order wide-angle parabolic equation (WAPE) approximation (Thomson and Chapman, 1983) can be used. It also features less sensitivity to the choice of k_o, and to the phase errors in typical deep ocean conditions, relative to the SPE approximation.(Jensen et al., 1994 and Chin-Bing et al., 1993)

The WAPE operators are defined as

$$T_{WAPE} \equiv -\frac{1}{k_o^2}\frac{\partial^2}{\partial z^2}\left[\left(1 + \frac{1}{k_o^2}\frac{\partial^2}{\partial z^2}\right) + 1\right]^{-1} \tag{10}$$

and

$$U_{WAPE} \equiv -(n - 1). \tag{11}$$

In order to numerically solve the parabolic equation, the MMPE uses the split-step Fourier (SSF) method. This algorithm integrates the solution in range by applying the operator U_{WAPE} in the z-domain., and the operator T_{WAPE} in the k_z-domain. The latter is defined, in the k_z-domain, as

$$\hat{T}_{WAPE}(k_z) \equiv 1 - \sqrt{\left(1 - \frac{k_z^2}{k_o^2}\right)} . \tag{12}$$

Note that both operators are just scalar multipliers, and may be applied independently.

The approximate solution for ψ is iterated in range according to the following expression

$$\psi(r + \Delta r, z) = e^{-ik_o \Delta r U_{WAPE}(r, z)} FFT\left(e^{-ik_o \Delta r \hat{T}_{WAPE}(r, k_z)}[FFT(\psi^*(r, z))]^*\right), \qquad (13)$$

where the FFT calculation is consistent with the form described in (Press et al., 1988). A forward FFT and double conjugation emulate the inverse FFT. The model outputs the field functions ψ (both magnitude and phase), referenced to a unit magnitude at r = 1m, and computed at the spatial grid points.

The source assumed in our model had a 600 Hz bandwidth centered at 900 Hz. Therefore, the acoustic field was computed for each one of the discrete frequencies (N=512) of the considered BW, and the model properly represented the broadband acoustic field.

As the single component of the general field can be expressed as Eq. 5, and assuming a windowed (Hanning), normalized source amplitude, the time-domain complex pressure field can be written as

$$p(r, z, t) = \int_{-\infty}^{\infty} p(r, z, f) e^{-i2\pi f t} df$$

$$= \frac{1}{\sqrt{r}} \int_{-\infty}^{\infty} e^{ik_o r} \psi(r, z, f) e^{-i2\pi f t} df \quad . \qquad (14)$$

13

Note that the overall phase factor $e^{ik_o r} = e^{i2\pi f\frac{r}{c_o}}$ can be neglected if we consider that the

arrival times are given in terms of "reduced time" $T = t - \left(\dfrac{r}{c_o}\right)$, then

$$p(r, z, T) = \frac{1}{\sqrt{r}} \int_{-\infty}^{\infty} \psi(r, z, f) e^{-i2\pi fT} df. \qquad (15)$$

This means that the time domain is heterodyned around $t = \dfrac{r}{c_o}$, and the use of a reduced

time does not have any influence on the autocorrelation function. The model also

heterodynes the signal by shifting the center frequency to zero (d.c.), in order to reduce the

computational load associated with large transform sizes. This procedure does not

introduce any consequence to our algorithm.

The MMPE model, a FORTRAN® code, is the latest version of what was formerly

known as the University of Miami Parabolic Equation (UMPE) model (Smith and Tappert,

1993). It requires a series of input files with strict formats, which properly represent:

- environmental data (sound-speed profile, bathymetry of water/bottom interface, bathymetry of the deep layer beneath the water/sediment interface, acoustic parameters of this "deep" layer, and acoustic parameters of the medium just below the water/bottom interface);

- source data, with two types available, wide-angle and vertical line array (steering allowed). We only used the wide-angle, which approximates the point source. The center frequency, bandwidth, and number of discrete frequencies (a power of two, because of the FFT) are also required.

All these input files are specified in a main one, the "pefiles.inp", where several other data

(name of output files, grid size and grid steps, c_0, size of vertical FFT, etc.) are contained.

14

The output is presented in a single binary file composed of a header (with the information needed for post-processing), and the complex PE field function ψ at selected grid points for every discrete frequency.

III. THE FREQUENCY-DOMAIN AUTOCORRECTION MATCHING (FACM) LOCALIZATION ALGORITHM

The algorithms studied in the Transient Localization Project at Naval Postgraduate School are designed for data from a single receiver hydrophone and a point source. The basic concepts of the correlation functions are outlined in Bendat and Piersol (1971), and the routines are described in Miller et al. (1996), Pierce (1996), and Hager (1997). From Brune (1998) we have that:

> Localization algorithms may be considered generalized beamformers in which the plane wave replicas have been replaced by more complicated replicas of the acoustic propagation (e.g., modes, beams, or the vertical pressure field). The algorithms, usually referred to as processors, are in most cases based on a Hermitian quadratic product. The exact form is determined by the constraints that are put on the processor output.

As discussed in Chapter II, replicas are simulated received signals of synthetic sources located at the points of a search grid. Generated by a propagation model, they are matched with the received signal. Considering that the source functions are equal and a perfect model is used, the exact match should occur where real and synthetic source locations coincide. An ambiguity surface usually represents the localization algorithm results.

The reciprocity principle states that, in a time-invariant and homogeneous environment, the acoustic pressure at location A due to an omnidirectional source located in B is equivalent to that of location B due to an omnidirectional source located in A. Using this principle, we reduce the computational load required to obtain localization,

since we are able to set the propagation model to generate replicas from the receiver position to all source possible locations in the grid.

In this chapter, we discuss the derivation of the frequency-domain autocorrelation matching (FACM) localization algorithm. Autocorrelation matching was originally designed for use in the time-domain (TACM), therefore it is more convenient to start its study treating the problem in time, and then to convert the results to the frequency domain. Previous investigations done by de Kooter (1997) showed that the TACM algorithms present very small footprints and large phase errors at higher frequencies, being useful for very low frequency signals. It was also observed that matching the time-domain amplitude-squared signals, which seemed relatively similar, could be more effective and robust. Therefore, as we will describe in the following paragraphs, an almost natural further development led to the frequency-domain algorithm. We begin with a complex pressure time series P(t), which represents a detected transient arrival.

The signal autocorrelation in the time-domain can be expressed by

$$T_{PP}(\tau) = \int_{-\infty}^{\infty} P^*(t)P(t+\tau)dt \qquad (16)$$

or, in terms of the frequency-domain response, by

$$T_{PP}(\tau) = \int_{-\infty}^{\infty} \tilde{P}^*(f)\tilde{P}(f)e^{-i2\pi f\tau}df, \qquad (17)$$

where

$$\tilde{P}(f) = \int_{-\infty}^{\infty} P(t)e^{i2\pi ft}dt. \qquad (18)$$

Then, the normalized autocorrelation becomes

$$C_{PP}(\tau) = \frac{T_{PP}(\tau)}{\int_{-\infty}^{\infty} \left|\tilde{P}(f)\right|^2 df} .$$ (19)

A similar derivation applied to the predicted replica signal R(t) leads to

$$C_{RR}(\tau) = \frac{T_{RR}(\tau)}{\int_{-\infty}^{\infty} \left|\tilde{R}(f)\right|^2 df} .$$ (20)

The autocorrelation matching algorithm is based upon the inner product of these two quantities and, normalized, in time-domain, it can be expressed by

$$A_{RP} = \frac{\int_{-\infty}^{\infty} C_{RR}^{*}(\tau) C_{PP}(\tau) d\tau}{\left[\int_{-\infty}^{\infty} \left|C_{RR}(\tau)\right|^2 d\tau \int_{-\infty}^{\infty} \left|C_{PP}(\tau)\right|^2 d\tau\right]^{1/2}} .$$ (21)

By analogy, in the frequency-domain it becomes

$$\tilde{A}_{RP} = \frac{\int_{-\infty}^{\infty} \tilde{C}_{RR}^{*}(\phi) \tilde{C}_{PP}(\phi) d\phi}{\left[\int_{-\infty}^{\infty} \left|\tilde{C}_{RR}(\phi)\right|^2 d\phi \int_{-\infty}^{\infty} \left|\tilde{C}_{PP}(\phi)\right|^2 d\phi\right]^{1/2}} ,$$ (22)

where $\tilde{C}_{PP}$ and $\tilde{C}_{RR}$ are the autocorrelations in frequency-domain of the transient signal and of the replica, respectively.

Since

$$\int_{-\infty}^{\infty} \tilde{C}_{RR}^{*}(\phi)\tilde{C}_{PP}(\phi)d\phi= \int_{-\infty}^{\infty} d\phi\left[\int_{-\infty}^{\infty} dt|R(t)|^2 e^{i2\pi\phi t}\right]\left[\int_{-\infty}^{\infty} dt'|P(t')|^2 e^{i2\pi\phi t}\right]$$

$$= \int_{-\infty}^{\infty} dt'|P(t')|^2\int_{-\infty}^{\infty} dt|R(t)|^2\left[\int_{-\infty}^{\infty} d\phi e^{i2\pi\phi(t'-t)}\right] \qquad (23)$$

$$= \int_{-\infty}^{\infty} |R(t)|^2|P(t)|^2 dt$$

Eq. 22 can be rewritten as

$$\tilde{A}_{RP} = \frac{\displaystyle\int_{-\infty}^{\infty} |R(t)|^2|P(t)|^2 dt}{\left[\displaystyle\int_{-\infty}^{\infty} |R(t)|^4 dt\int_{-\infty}^{\infty} |P(t)|^4 dt\right]^{1/2}}. \qquad (24)$$

In order to reduce the influence of noise, we shall remove the zero-lag component of the autocorrelation function, which is equivalent to removing the mean of the squared amplitude of the time-domain signal. Therefore, we define

$$|R'(t)|^2 = |R(t)|^2 - \langle|R(t)|^2\rangle_t \qquad (25)$$

and

$$|P'(t)|^2 = |P(t)|^2 - \langle|P(t)|^2\rangle_t, \qquad (26)$$

where $< >_t$ is an average over all times. Eq. 24 then becomes

$$\tilde{A}_{RP} = \frac{\displaystyle\int_{-\infty}^{\infty} |R'(t)|^2|P'(t)|^2 dt}{\left[\displaystyle\int_{-\infty}^{\infty} |R'(t)|^4 dt\int_{-\infty}^{\infty} |P'(t)|^4 dt\right]^{1/2}} \qquad (27)$$

which is focused on the influence of matching the non-zero lag components.

However, it still presents an ambiguity in (absolute) time which was not present in TACM, and we shall introduce a search parameter τ to allow us to slide the replica signal in time, searching for the optimal match. The FACM function then becomes

$$\tilde{A}_{RP} = \max_{\tau}\left\{\frac{\int_{-\infty}^{\infty}|R'(t+\tau)|^2|P'(t)|^2dt}{\left[\int_{-\infty}^{\infty}|R'(t)|^4dt\int_{-\infty}^{\infty}|P'(t)|^4dt\right]^{1/2}}\right\}, \tag{28}$$

where max_{τ} is the maximum value of the function for any value of the search parameter τ.

A MATLAB$^{\circledR}$ implementation of the algorithm based on Eq. 28 was used to generate all the ambiguity surfaces shown in this work. The sliding-τ operation was performed according to the following development. Let $g(t) \equiv |P'(t)|^2$ and $h(t) \equiv |R'(t)|^2$, then

$$g(t) = \int_{-\infty}^{\infty}e^{-i2\pi ft}G(f)df, \tag{29}$$

and

$$h(t) = \int_{-\infty}^{\infty}e^{-i2\pi ft}H(f)df$$

$$h(t+\tau) = \int_{-\infty}^{\infty}e^{-i2\pi f(t+\tau)}H(f)df = \int_{-\infty}^{\infty}e^{-i2\pi ft}H(f)e^{-i2\pi f\tau}df. \tag{30}$$

Therefore, the numerator of Eq. 28 becomes

$$A(\tau) = \int_{-\infty}^{\infty} h(t+\tau)g(t)dt. \tag{31}$$

If *h(t)* is a real function,

$$A(\tau) = \int_{-\infty}^{\infty} h^*(t+\tau)g(t)dt$$

$$= \int_{-\infty}^{\infty}\left[\int_{-\infty}^{\infty} e^{i2\pi ft}H^*(f)e^{i2\pi f\tau}df\right]\left[\int_{-\infty}^{\infty} e^{-i2\pi f' t}G(f')df'\right]dt$$

$$= \int\int_{ff'}\left[H^*(f)G(f')e^{i2\pi f\tau}\int_{-\infty}^{\infty} e^{-i2\pi(f'-f)t}dt\right]df'df$$

$$= \int_{-\infty}^{\infty} H^*(f)G(f)e^{i2\pi f\tau}df \quad, \tag{32}$$

knowing that

$$\int_{-\infty}^{\infty} e^{-i2\pi(f'-f)t}dt = \delta(f'-f). \tag{33}$$

Hence, the search over τ was in fact computed by a multiplication in the frequency domain and an inverse FFT operation represented by the numerator $A(\tau)$. Prior investigations (Brune, 1998 and de Kooter, 1997) had shown that the FACM algorithm is better suited for larger bandwidths and higher frequencies, when compared to its analog in

the time domain, the TACM algorithm. Also, FACM is more robust against environmental

mismatch and presents better peak-to-sidelobe levels and larger footprints.

IV. SIGNAL PROCESSING AND ENVIRONMENTAL ASSESSMENTS

A. MATCHED-FILTER PROCESSING

Matched filtering (MF) is a process where the received signal r(t) is correlated against a replica of the transmitted signal s(t), in order to obtain a better signal-to-noise ratio (SNR) and reduce the effective temporal structure of the source down to an ideal, coherent pulse. It is also known as a conjugate filter, since its frequency response is basically the conjugate of the (transmitted) signal spectrum (Tolstoy, A., 1993). In this work, matched-filtering was used first to identify the short duration bursts (0.1s) in the 2-min. long data files. Second, but more importantly, to process the bursts and obtain data emulating the existence of a coherent source, instead of the actual non-coherent one. This also provides a baseline for the localization results since the model-generated replicas are based on a coherent source. Therefore, this is equivalent to localizing a transient with known source function.

The process was implemented digitally in MATLAB®, according to the expression

$$p(t) = \int_{-\infty}^{\infty} S^*(f)R(f)e^{i2\pi ft}df, \tag{34}$$

where $p(t)$ is the matched-filtered output in time-domain, $S^*(f)$ is the complex conjugate of the transmitted signal in the frequency domain, and $R(f)$ is the received signal in the frequency domain.

An example of the MF output in time domain can be visualized in Figure 4.1, and its frequency spectrum in Figure 4.2. The raw data is also shown and, by comparison, we can observe the significant noise reduction.
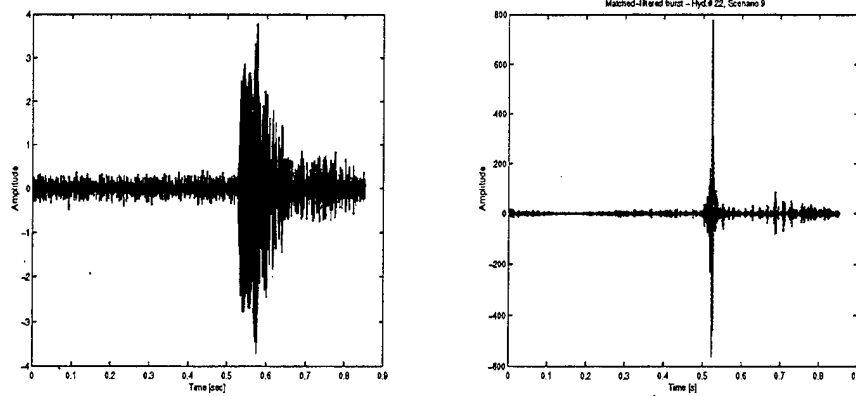

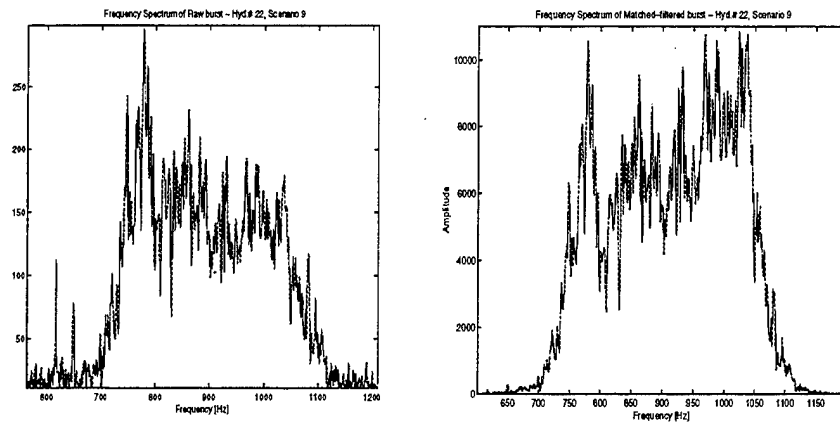Figure 4.1. Examples of a Raw (Left) and an MF Burst (Right) in the Time-Domain.

Figure 4.2. The Frequency Spectra of a Raw Burst (Left) and of an MF Burst (Right).

B. PLANE-WAVE BEAMFORMING

Plane-wave beamforming is one of the many techniques used to distinguish particular features of a received signal while reducing the influence of noise - which is usually generated near the surface, and tends to occur in high modes or high angles of propagation (Jensen et al., 1994). It consists of decomposing the signal into plane waves by summing the outputs of spatially distributed sensors - in this work, eight hydrophones for each of the three sub-arrays in the VLA.

In underwater acoustic propagation, much of the information about the environment and the relative source/receiver location is contained in the vertical structure of the acoustic field. Therefore, the ability to resolve the vertical structure of the arrival at the receiver can lead to estimations of the corresponding source location.

A beamformer is especially useful because it allows us to give preference to one direction of propagation over another, implementing a spatial filter. In this work, it was used to observe the dominant beams when the signal was arriving at the VLA, providing information for a comparison of the localization algorithm results by the distinct arrival angle structures.

An excellent discussion about the beamforming process is presented by Defatta et al., (1988) and its summary follows. Consider an infinite, homogeneous medium containing a line array of equally spaced elements positioned along the y-axis, and an undetermined number of remote sources. The output of an element located at the origin of coordinates

due to the lth source is defined as $S_l(t)$. Assuming plane-wave propagation in the far-field, a source from direction θ_l outputs

$$e_n(t) = S_l\left(t + \frac{nd\sin(\theta_l)}{c}\right), \tag{35}$$

where n is the array element index, d is the spacing of the elements, θ_l is the angle of arrival from the lth source, and c is the speed of propagation. To accomplish beamforming, we must apply weights θ_m and time delays to the individual element signals, and then coherently sum them. Therefore, the output of the beamformer in the direction θ_m is

$$b_m(t) = \sum_{n=0}^{N-1} w_l S_l\left\{t + \frac{nd[\sin(\theta_l) - \sin(\theta_m)]}{c}\right\}. \tag{36}$$

To derive the directional response characteristics of the beamformer, we shall consider a continuous, complex plane-wave signal propagating across the array,

$$S_l = e^{i\omega_l t}. \tag{37}$$

Due to the arrival angle θ_l, the sensor outputs

$$e_n(t) = e^{i\omega_l t} e^{ink_l d\sin(\theta_l)}, \tag{38}$$

where $k_l = \frac{2\pi}{\lambda_l} = \frac{\omega_l}{c}$ is the wave number of the lth source.

28

The beamformer output is then

$$b_m(t) = e^{i\omega_l t} \sum_{n=0}^{N-1} w_n e^{ink_l d[\sin(\theta_l) - \sin(\theta_m)]} = W(\theta_l) e^{i\omega_l t}, \tag{39}$$

where

$$W(\theta_l) = \sum_{n=0}^{N-1} w_n e^{ink_l d[\sin(\theta_l) - \sin(\theta_m)]} \tag{40}$$

is the spatial Fourier transform of the array weights.

The beamforming operation applied in this work was implemented using FFT in MATLAB®. Single frequencies considered, the time-delay operations described above are equivalent to phase shifts that are linear functions of the element index. FFT beamforming is the implementation of these phase shifts through FFT operations. The processed results for all three sub-arrays, and the three distinct scenarios can be seen in Figures 4.3, 4.4, and 4.5. They describe the physical angle of arrival as a function of the reduced time, and provide an easy visualization of the multipath nature of the burst propagation. The results for sub-array 2, however, are noticeably affected by the lack of data from hydrophones 17 and 18. We can verify in Figure 4.3 (scenario 11, range ~500 m) that the energy is not as concentrated in the lower angles as in the other two figures corresponding to larger ranges. However, in all of them we observe the early arrivals of the lower angles, the short period in which the energy is contained, and the distinct multipath structure.
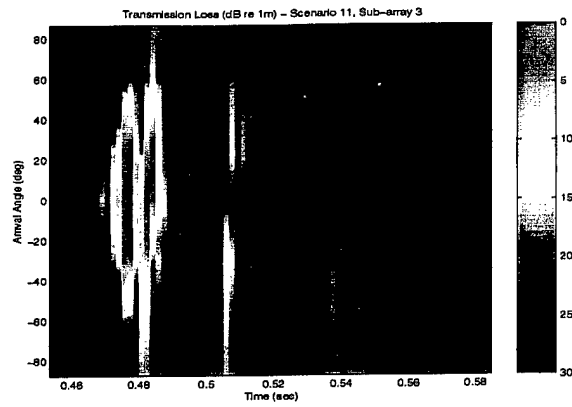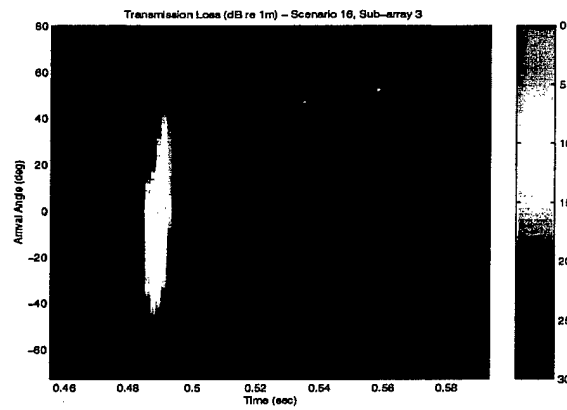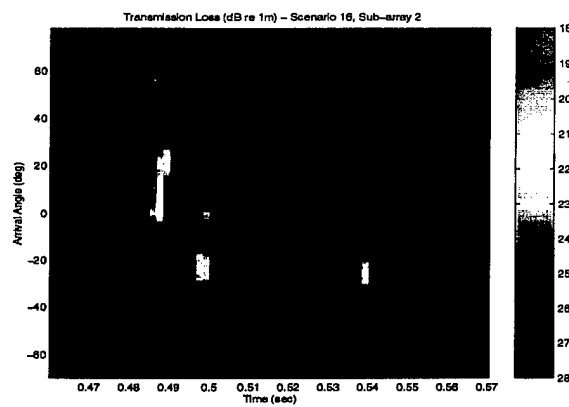
(a) Sub-array 3
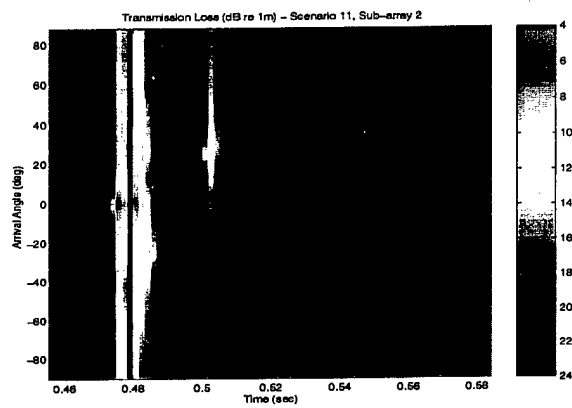
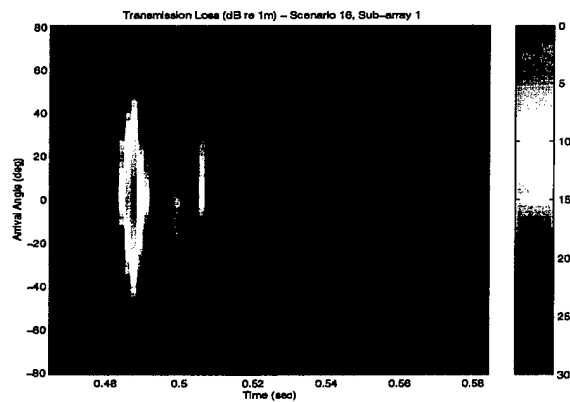(b) Sub-array 2
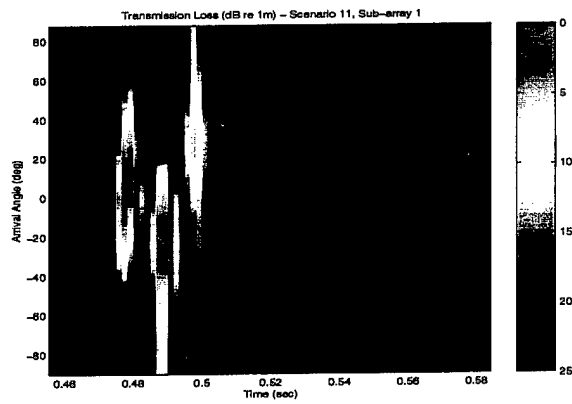
(c) Sub-array 1

Figure 4.3. Beamformer Outputs for Scenario 11 (Range 460 m, Depth 45.7 m).
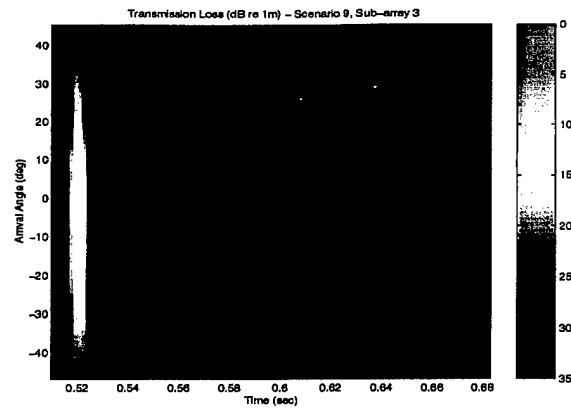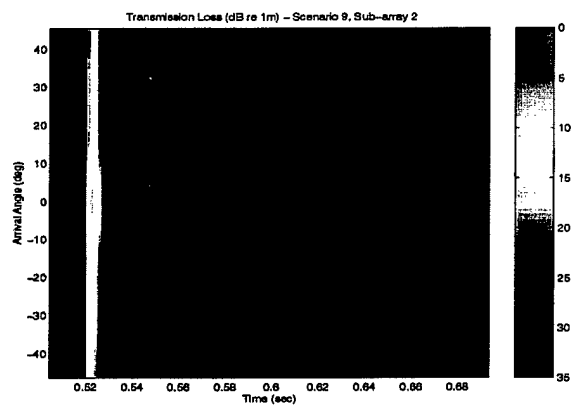
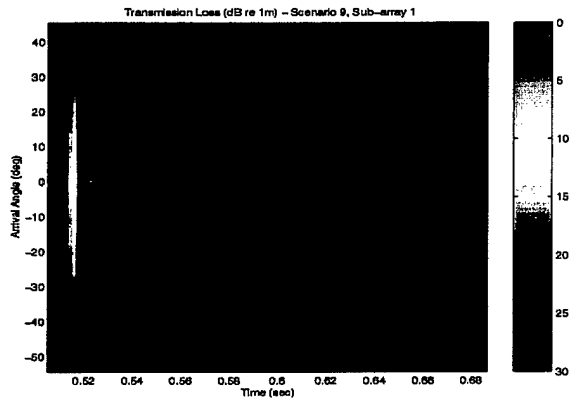(a) Sub-array 3

(b) Sub-array 2

(c) Sub-array 1

Figure 4.4. Beamformer Outputs for Scenario16 (Range 2194 m, Depth 27.4 m).

31

(a) Sub-array 3

(b) Sub-array 2

(c) Sub-array 1

Figure 4.5. Beamformer Outputs for Scenario 9 (Range 4650 m, Depth 45.7 m).

C. MODAL ANALYSIS

Normal modes are another physical, frequency-dependent representation of the underwater acoustic wavefield. For a given sound channel, the acoustic modes represent a unique, natural set of standing waves oscillating along the depth axis (Chiu and Ehret, 1994).

The method involves solving a depth-dependent equation, and the complete acoustic field is then constructed by summing up contributions of each of the modes weighted in accordance to the source depth. The modal equation

$$\rho(z)\frac{d}{dz}\left[\frac{1}{\rho(z)}\frac{d\Psi_m(z)}{dz}\right] + \left[\frac{\omega^2}{c^2(z)} - k_{rm}^2\right]\Psi_m(z) = 0 , \tag{41}$$

with boundary conditions $\Psi(0) = 0$ (pressure-release surface at z=0) , and $\left.\frac{d\Psi}{dz}\right|_{z=D} = 0$

(perfectly rigid bottom at z = D) is a classical *Sturm-Liouville* eigenvalue problem, whose properties are well known (if we assume that $\rho(z)$ and $c(z)$ are real). Some are:

- the modal equation has an infinite number of solutions which are like the modes of a vibrating string;

- the modes are characterized by a mode shape function $\Psi_m(z)$ (an *eigenfunction*) and a horizontal propagation constant *krm (eigenvalues)*. These constants are all distinct and analogous to a frequency of vibration; and

- the modes are unique (orthogonal) and form a complete set, which means that we can represent an arbitrary function as a sum of the normal modes.

Based upon these and through a modal decomposition implemented in MATLAB, we were able to quantify the amplitudes of the first 30 modes as functions of the signal (discrete) frequencies and, by IFFT, of the reduced time. The SSP's used were the ones discussed in Chapter I and depicted in Figure 1.6, applied to their respective cases. A visualization of the first ten modes of the assumed waveguide for a frequency f = 900 Hz is presented in Figure 4.6. The final results of the modal decomposition of the received signal for each studied scenario are shown in Figures 4.7, 4.8 and 4.9. Note the energy concentration in the lower modes, especially scenarios 9 (5000 m) and 16 (2500 m). This is consistent with stripping of higher modes at longer ranges. The energy observed in the higher modes must be treated with skepticism since the array does not sample those modes very well. The lack of tilt information in this analysis also makes the higher mode decomposition suspect.
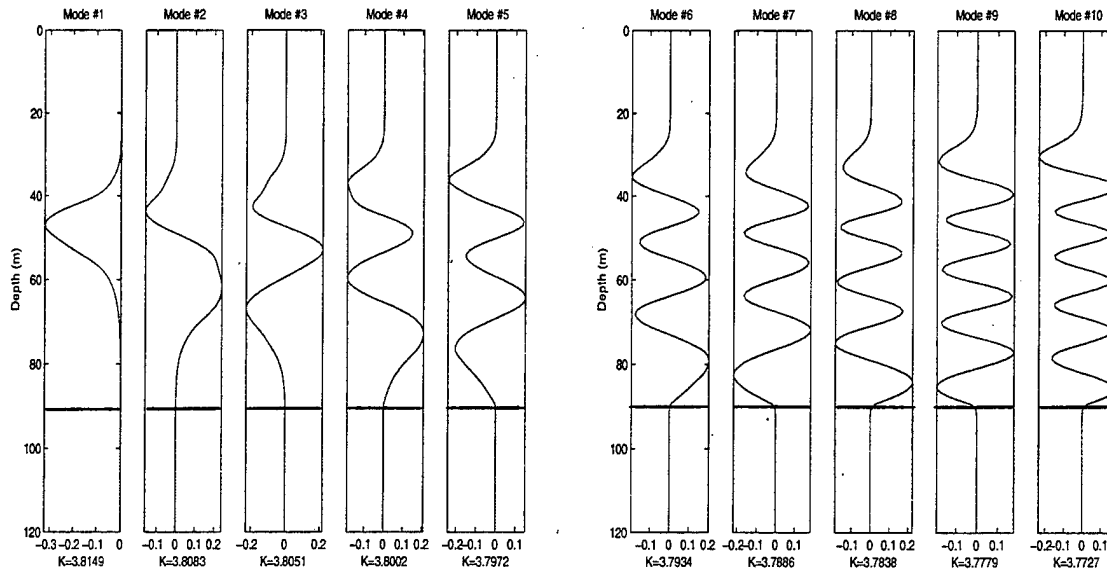

Figure 4.6. The First 10 Normal Modes (f = 900 Hz). The Bottom Depth is 89.9 m.
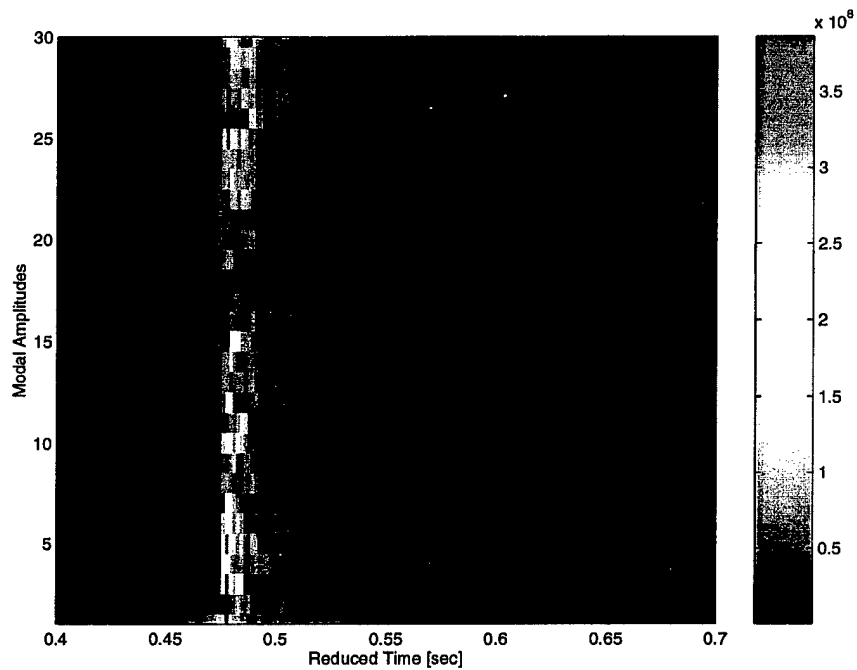
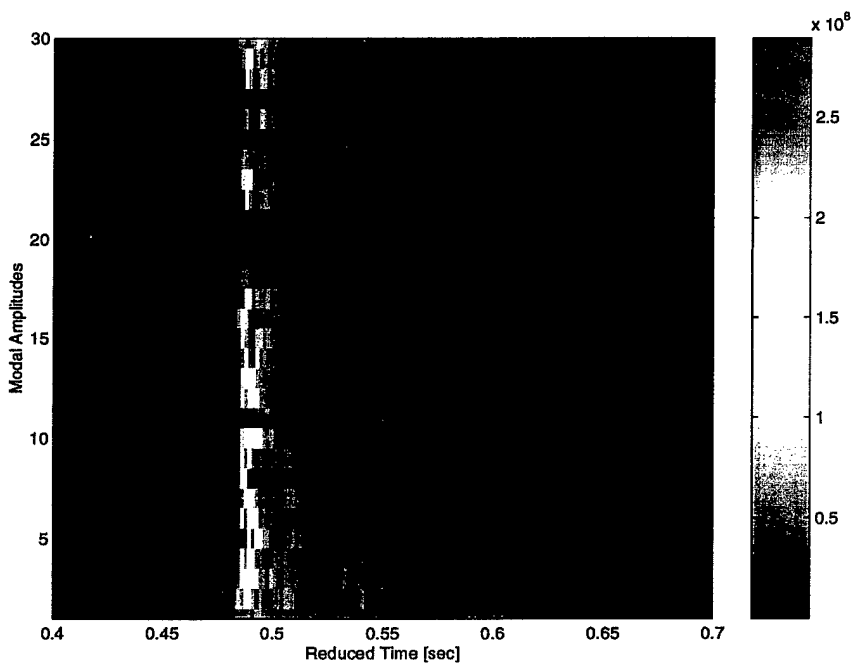Figure 4.7. Modal Amplitudes vs. Reduced Time - Scen.11 (Range 460 m, Depth 45.7 m).

Figure 4.8. Modal Amplitudes vs. Reduced Time-Scen.16 (Range 2194 m, Depth 27.4 m).
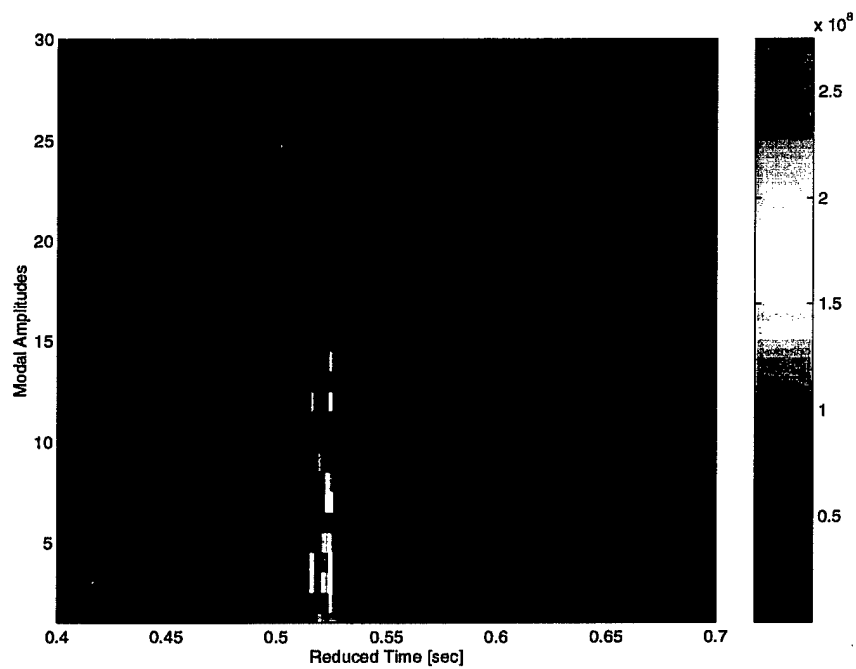
35

Figure 4.9. Modal Amplitudes vs. Reduced Time-Scen.9 (Range 4650 m, Depth 45.7 m).

D. SPATIAL COHERENCE (CORRELATION)

In order to analyze the spatial coherence of the signal's vertical structure at the VLA, single records from each of the three scenarios were considered. We computed the peak correlation of each phone's data with a reference phone (hyd #1, closer to the bottom; 16, mid-array; and 32, closer to the surface) normalized such that the autocorrelation of the reference phone data was unity. The results provided information about how unique the signal was across the space (vertical direction). We can observe in Figure 4.12, from scenario 9 (range ~5000 m), that the signal correlation decreases to values around 0.5 over about 5 meters in depth for the reference hydrophones 1 (bottom) and 32 (top), which corresponds to one element spacing and approximately two to four wavelengths. The same effect can be verified in Figure 4.11 which displays data from scenario 16 (range ~2500 m). These results suggest that distinct multipath arrivals at any given time are interacting at different locations over the array length. For scenario 11 (range ~500 m) runs, however, the cross-correlation is not as low for the same difference in depth, as shown in Figure 4.10. This is a consequence of the short distance between source and receiver which does not allow large variations in the signal nor many multipath arrivals. Also, by observing Figure 4.12, we notice that hydrophone 16's signals are more correlated than the ones from hydrophones 1 and 32 for scenario 9. This could be a consequence of its relative position (mid-array), but the same effect was not verified in scenarios 11 and 16.
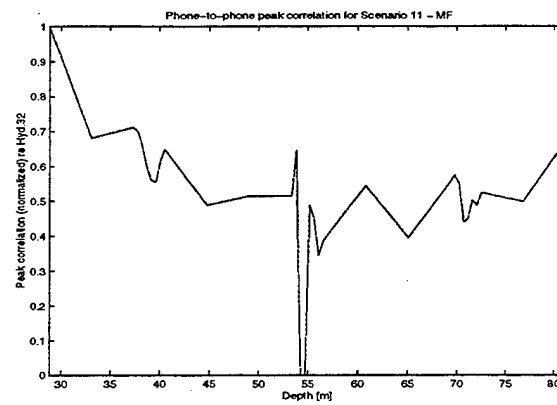
(a) Reference Hydrophone # 32 (Depth 28 m)
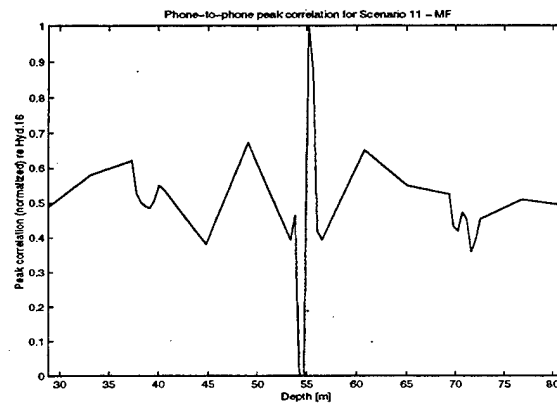
(b) Reference Hydrophone # 16 (Depth 54.8 m)
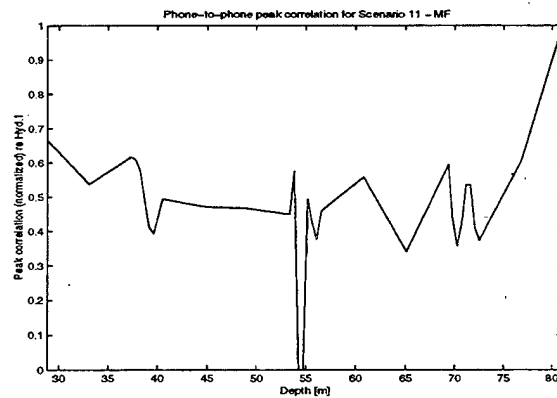
(c) Reference Hydrophone # 1 (Depth 82 m)

Figure 4.10. Phone-to-Phone Peak Correlation - Scenario 11 (Range 460 m).

(a) Reference Hydrophone # 32 (Depth 28 m)

(b) Reference Hydrophone # 16 (Depth 54.8 m)

(c) Reference Hydrophone # 1 (Depth 82 m)

Figure 4.11. Phone-to-Phone Peak Correlation - Scenario 16 (Range 2194 m).

(a) Reference Hydrophone # 32 (Depth 28 m)
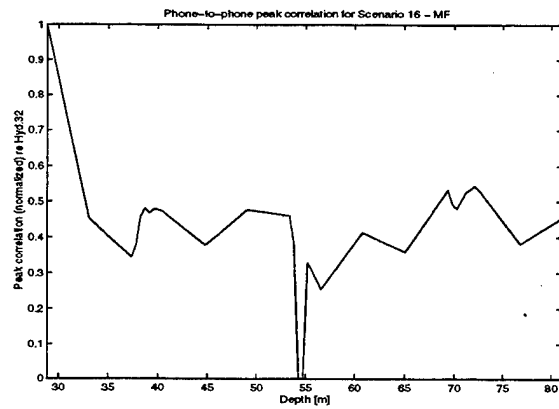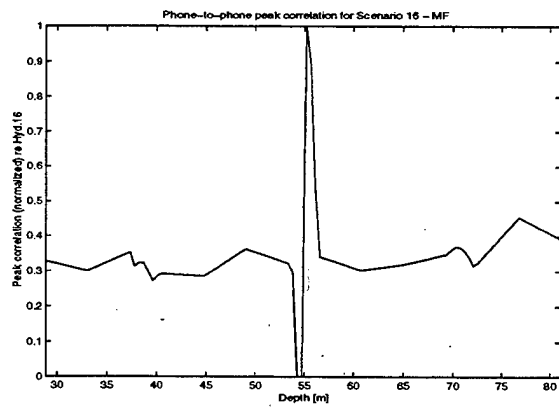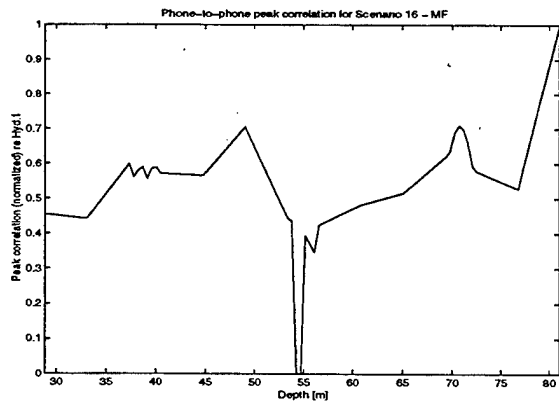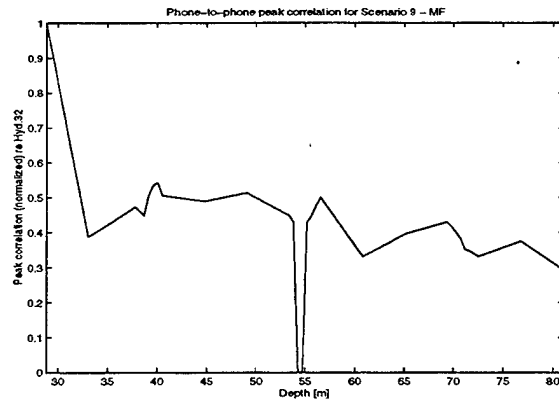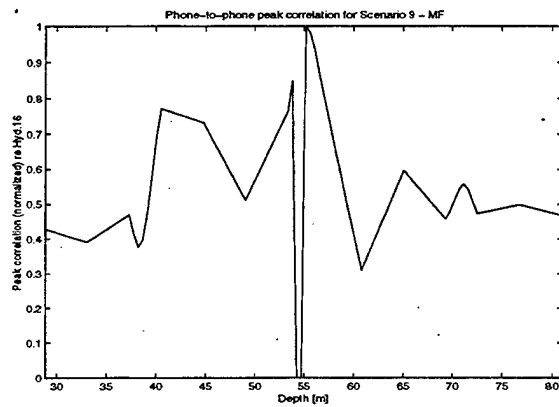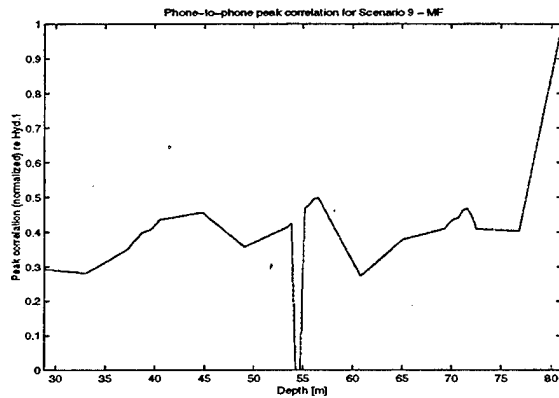

(b) Reference Hydrophone # 16 (Depth 54.8 m)

(c) Reference Hydrophone # 1 (Depth 82 m)

Figure 4.12. Phone-to-Phone Peak Correlation - Scenario 9 (Range 4960 m).

V. LOCALIZATION RESULTS

This chapter presents a compilation of results obtained after a series of runs of the FACM algorithm. For every scenario, distinct receiver depths were tested by selecting the hydrophone data to be used.

Regarding the environmental parameters used as inputs to the MMPE model, only the sound speed profile varied according to the respective scenario. We used only the bathymetry along the North radial, which is an approximate 89.9 m isobath with bottom composed mainly of medium to coarse grained sands. This type of sand has the following properties: compressional sound speed of ~1800 m/s, sound speed gradient of $25s^{-1}$, shear speed of ~250 m/s, density ~2.03 g/cm^3, and compressional and shear wave attenuation coefficients about 0.1 dB/m and 1.0 dB/m, respectively (Smith et al., 1998). During the experiment, the data was recorded at a sampling frequency of 4934.0 Hz. For processing, we extracted the received hydrophone response to the 0.1s bursts in files of 4210 points which corresponded to 0.8533 seconds. The reason for this procedure is that, in the MMPE model output, we have 512 discrete frequencies over a 600 Hz bandwidth. Therefore, $\Delta f = 1.171875\,\text{Hz}$, and we match $T = \dfrac{1}{\Delta f} = 0.8533$. After, we processed it again to reduce its length to 2048 spectral points over a bandwidth of 600 Hz to 1200 Hz. The model output was zero-padded (both ends) to also contain 2048 points.

The spatial grid was, in most of the runs, 128 points in depth vs. 300 points in range. In general, it corresponded to a resolution of 0.78 m in depth and 10 m in range. For all cases, the source/receiver relative position proved to be a very important factor to the quality of the results. This can be observed in Figures 5.1 (a) and (b), where the ambiguity surfaces for scenario 9, based on hydrophone 16 (a), and hydrophone 2 (b), are shown. The source is located at depth 45.7 m, range 4650 m, and its location is depicted as a white dot. While the algorithm with hydrophone 16 (depth = 54.8 m) data was able to localize it within the some tolerance, the run with hydrophone 2 (depth = 76.3 m) data did not provide localization at all.

By processing the matched filtered signal, we simulate the (idealistic) situation of a coherent source, and it improved the localization results a little. However, even when processing the raw data, we obtained satisfactory results where the main differences were the bigger footprint and the smaller values of the ambiguity surface. These differences can be observed in Figures 5.2, 5.3, and 5.4, which display results for scenario 9, scenario 16, and scenario 11, respectively.

Observing Figures 5.3(b) and 5.4(b), where the ambiguity surfaces from runs with MF data from scenarios 16 and 11 are shown, respectively, we verify that the FACM localization algorithm performed reasonably well (errors < 11% in range, and < 40% in depth). It is important to note that the sound speed profiles used were gathered four hours apart from experiments of scenario 9, more than two hours apart from scenario 11's, and

42

more than 10 hours apart from scenario 16's. The mismatch between the actual and the modeled environmental parameters contained in the SSP is likely significant.

We also observed that the localization error decreased with increasing range. This was expected since the autocorrelation techniques are strongly dependent on the uniqueness of the multipath structure. The error obtained for scenario 9 (range ~5000 m) runs were in the order of 2% in range and 30% in depth. However, scenario 11 (range ~500 m) runs presented errors as large as 20% in range and 40% in depth.
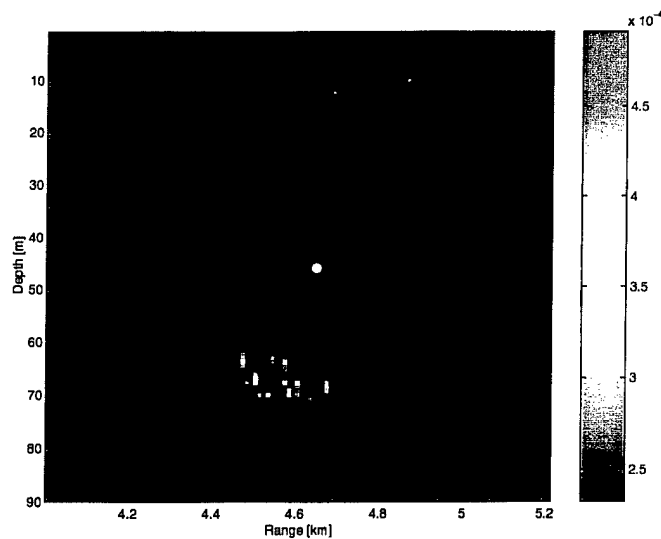
(a)
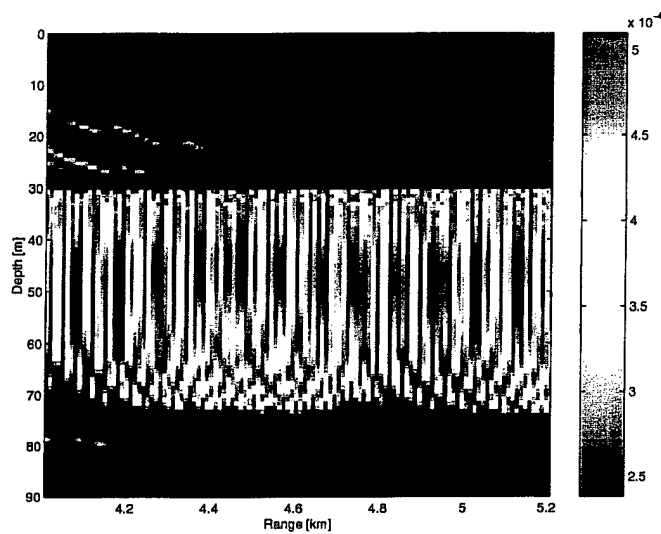
(b)

Figure 5.1. Ambiguity Surfaces for Scenario 9-(a) with Raw Data from Hyd.16 (Depth 54.8 m), and (b) with Raw Data from Hyd.2 (Depth 76.3 m). The White Dot Depicts the Actual Source Location.
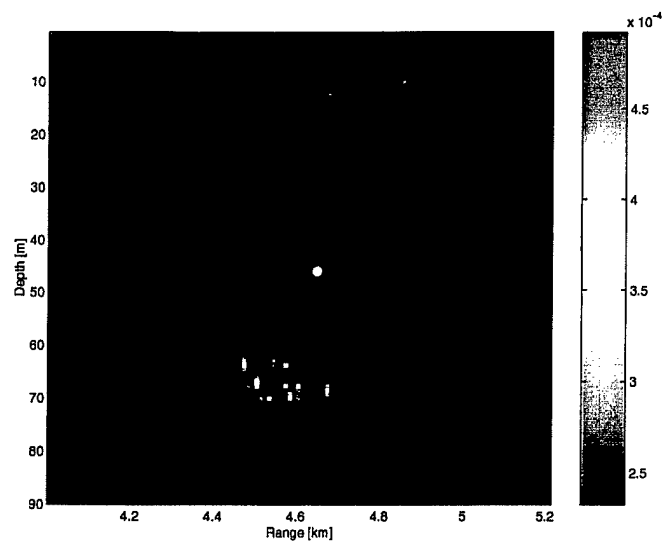
(a)
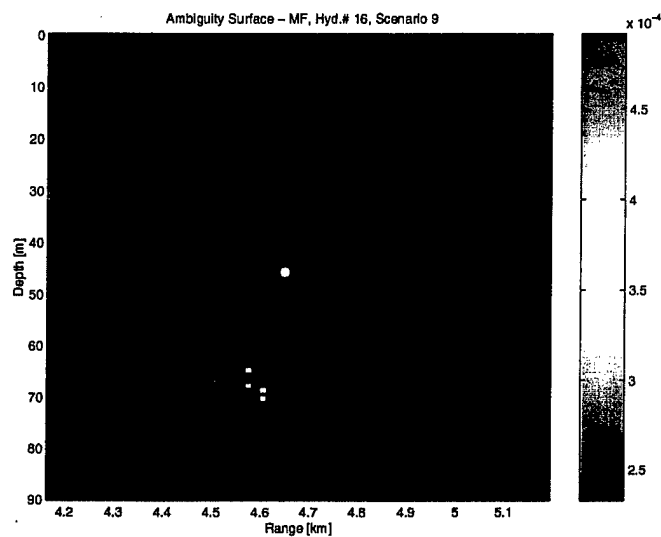
(b)

Figure 5.2. Ambiguity Surfaces for Scenario 9 - (a) with Raw Data and (b) with MF Data
from Hyd.16 (Depth 54.8 m).The White Dot Depicts the Actual Source Location.

(a)

(b)

Figure 5.3. Ambiguity Surfaces for Scenario 16- (a) with Raw Data and (b) with MF Data, both from Hyd. 16 (Depth 54.8 m).The White Dot Depicts the Actual Source Location.

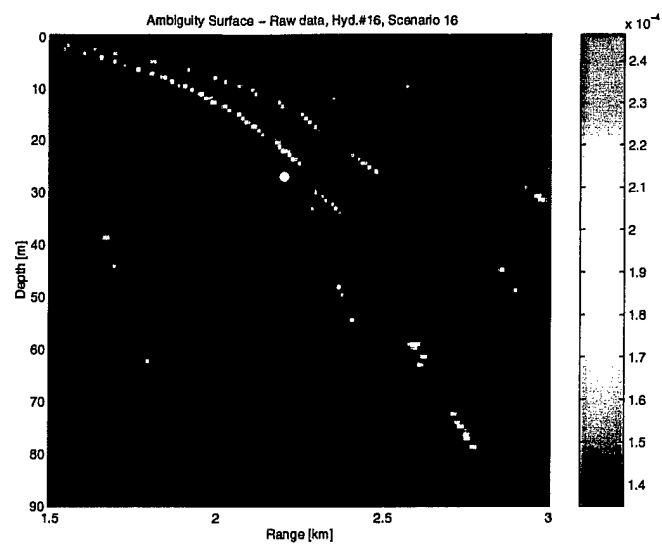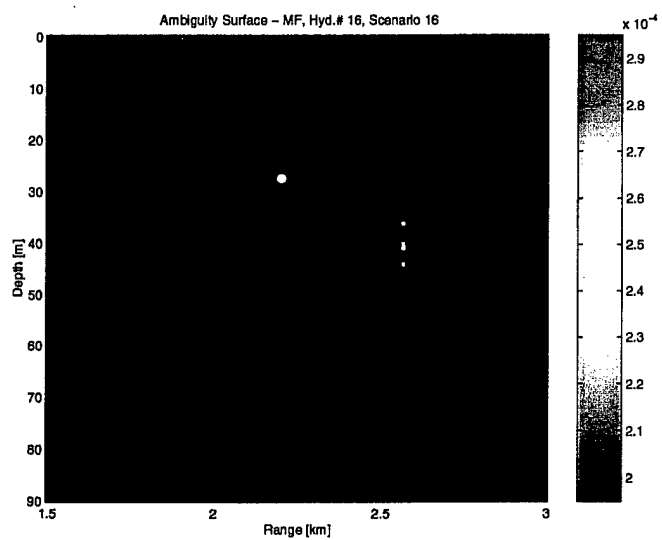**(a)**

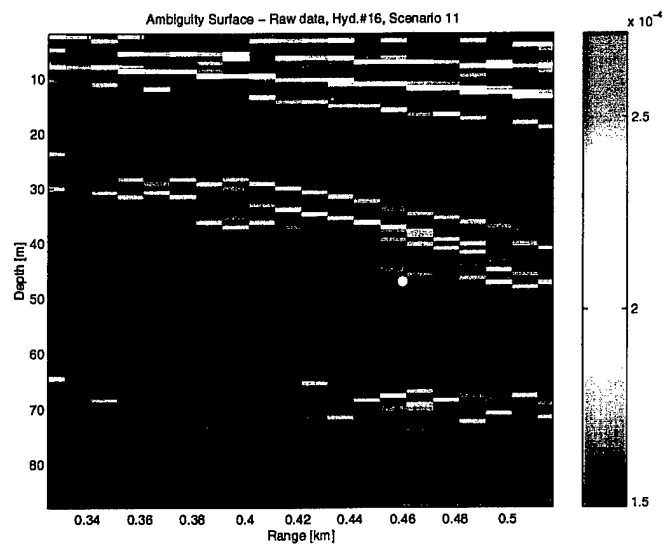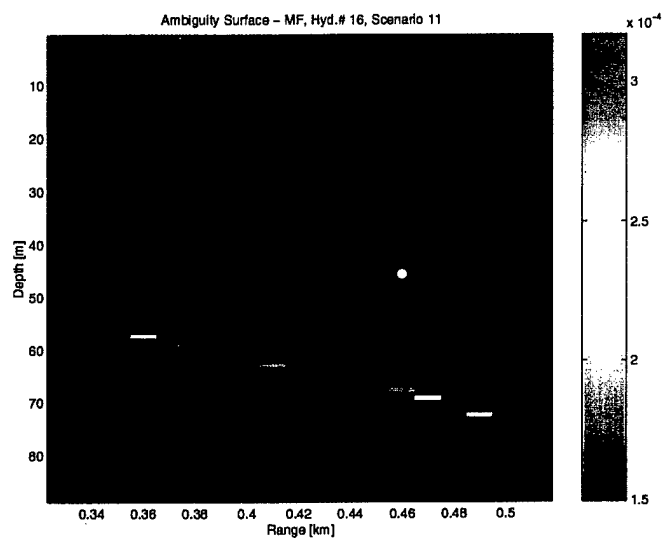**(b)**

Figure 5.4. Ambiguity Surfaces for Scenario 11- (a) with Raw Data and (b) with MF Data, both from Hyd. 16 (Depth 54.8 m).The White Dot Depicts the Actual Source Location.

VI. CONCLUSIONS

A. SUMMARY OF FINDINGS

Several techniques helped us to assess the properties of the acoustic field in which we were applying the localization algorithm and infer their influences on it. Through spatial coherence analysis, we were able to verify that more unique signals led to better localization results, therefore, ratifying Brune (1998). Analyzing the beamformer outputs, we can affirm that more stratified, discrete structures, corresponding to the larger distances between the source and receiver also provided better results. Observing the sound speed profiles, we identified a sound channel spanning from a depth of about 30 m to the bottom. With the modal decomposition, we verified that the lower modes, which were closer to the channel axis (~ 45 m), carried more energy. When selecting a receiver above this channel, we observed poor results without any match, and the best results corresponded to hydrophones positioned closer to the sound channel axis. Another important fact to note is that the depths where we obtained localizations corresponded to the ones containing larger amplitude modes, mainly modes two to six depending on the source frequency chosen to be sampled.

Regarding the use of matched-filtered or raw data as inputs to the FACM algorithm, our work suggests that it is not a major issue - one can have localization results applying raw data as useful as the ones from MF data. However, these results were based solely on

LFM chirp transmissions and may not apply to all signals generally. Further studies are needed to examine this issue more thoroughly.

B. RECOMMENDATIONS FOR FUTURE WORK

Once we have data from 30 of the 32 hydrophones in the VLA, an almost natural consideration would be the multiple-phone analysis of the localization algorithms. While computational load would certainly be an issue, the comparison with single-phone analysis, and possibly better results, would be worth it. In this case, one should consider the use of the array tilt information contained in the data files to correct the arrival angle, vertical structure, hydrophone depth, etc.

Another possible approach would be the use of non-traditional processes, such as artificial neural networks (ANN) and minimum-variance spectrum estimations (MVSE), both in the arrival structure analysis and in the data preprocessing. This could surpass the over-simplifications of the traditionally used techniques and lead to better results (Ma, Y.L., 1997). Also, since the shallow water environment is generally a dispersive channel, and presents effects such as strong bottom reverberation, signal distortion and noise fluctuation, an analysis of the signal mismatch influences could introduce improvements to the process.

Throughout this work, only three scenarios were considered. As the NUWC-TSP experiment provided at least 14 other sets of data where parameters such as source location, signal bandwidth, and/or pulse duration differed from the ones we studied, it could be useful to process them to try to confirm our results. Moreover, it would allow a comparison of the FACM performance for longer pulses and higher frequencies.

LIST OF REFERENCES

Bendat, J. S. and Piersol, A. G., *Random Data: Analysis and Measurement Procedures*, Wiley-Interscience, New York, 1971.

Brune, J., "Transient Localization in Shallow Water Environments," Master's Thesis, Naval Postgraduate School, March 1998.

Chin-Bing, S. A., King, D. B., Davis, J. A., and Evans, R. B., eds., "Lloyd's Mirror – Wide Angle Propagation," in *PE Workshop II: Proceedings of the Second Parabolic Equation Workshop,* Naval Research Laboratory NRL/BE/7181-93-0001 (US Government Printing Office, pp. 62-67, 1993.

Chiu, C.-S., and Ehret, L. L., "Three-Dimensional Acoustic Normal Mode Propagation in the Gulf Stream," in *Oceanography and Acoustics: Prediction and Propagation Models*, p.179, edited by A. R. Robinson and D. Lee, American Institute of Physics Press, Woodbury, NY, 1994.

Chiu,C.-S., Apel, J. R., Badiey, M., Finette, S., Headrick, R., Kemp, J., Lynch, J. F., "An Overview of the 1995 SWARM Shallow-Water Internal Wave Acoustic Scattering Experiment," *IEEE Journal of Oceanic Engineering*, July 1997.

Defatta, D J., Lucas, J. G., and Hodgkiss, N. S., *Digital Signal Processing: A System Design Approach,* John Wiley and Sons, pp. 628-649, New York, NY, 1988.

Gradshteyn, I. S., and Ryzhik, I. M., *Table of Integrals, Series and Products*, Academic Press, Inc., pp.966 and 972, 1994.

Hager, C. A., "Modeling the performance of the Pt.Sur Hydrophone Array in Localizing Blue Whales," Master's Thesis, Naval Postgraduate School, September 1997.

Hardin, R. H., and Tappert, F. D., "Applications of the split-step Fourier method to the numerical solution of nonlinear and variable coefficient wave equations," SIAM Rev.15, p. 423, 1973.

Jensen, F. B., Kuperman, W. A., Porter M. B. and Schmidt H., *Computational Ocean Acoustics*, American Institute of Physics Press, Woodbury, NY, 1994.

de Kooter, P. M., "Variations on Autocorrelation Matching and the SIFT Localization Algorithm," Master's Thesis, Naval Postgraduate School, March 1997.

Ma, Y. L., "Emerging Issues in Underwater Acoustics Signal Processing for Shallow Water Environment," in *Shallow-Water Acoustics,"* pp. 535-537, edited by R. Zhang and J. Zhou, China Ocean Press, Beijing, PRC, 1997.

Miller, C. W., "Estimating the Acoustic Modal Arrivals Using Signals Transmitted From Two Sound Sources to a Vertical Line Hydrophone Array in the 1996 Shelfbreak Primer Experiment," Master's Thesis, Naval Postgraduate School, June 1998.

Miller, J. H., Benson, J. L., Chiu, C.-S., and Smith, K .B., *Transient Localization Project at the NPS*, Technical Report, Naval Postgraduate School, April 1996.

Pierce, D. D., "Range-Dependent Passive Source Localization using data from the Barents Sea Tomography experiment, Ph.D. Dissertation, " Naval Postgraduate School, June 1996.

Press, W. H., Flannery, B. P., Teukolsky, S. A., And Vetterling, W. T., *Numerical Recipes*, Cambridge University Press, New York, NY, 1988.

Smith, K. B., Personal communication, Naval Postgraduate School, April 1996. The Monterey-Miami Parabolic Equation (MMPE) model is an upgraded version of the University of Miami Parabolic Equation (UMPE) model (Smith and Tappert, 1993).

Smith, K. B., and Tappert, F. D., "UMPE: The University of Miami Parabolic Equation Model, Version 1.0," Marine Physical Laboratory Technical Memo 432, 1993.

Smith, K. B., Rojas, J. G., Miller, J. H., and Potty, G., "Geoacoustic Inversions In Shallow Water Using Direct Methods and Genetic Algorithm Techniques," *Proceedings of the Pacific Ocean Remote Sensing Conference (PORSEC '98)*, pp. 703-707, Qingdao, PRC, July 1998.

Tappert, F. D., "The parabolic approximation method," in *Lecture Notes in Physics*, Vol.70, Wave Propagation and Underwater Acoustics, pp. 224-287, edited by J.B. Keller and J.S. Papadakis, Springer Verlag, New York, NY, 1977.

Thomson, D. J., and Chapman, N. R., "A wide-angle split step algorithm for the parabolic equation models," *JASA Suppl.* 1 83, 1983.

Tolstoy, A., *Matched Field Processing For Underwater Acoustics*, p. 7, World Scientific, River Edge, NJ, 1993.

INITIAL DISTRIBUTION LIST

1. Defense Technical Information Center 2
   8725 John J. Kingman Rd., STE 0944
   Ft. Belvoir, VA 22060-6218

2. Dudley Knox Library 2
   Naval Postgraduate School
   411 Dyer Rd.
   Monterey, CA 93943-5101

3. Prof. Kevin B. Smith 5
   Physics Department, Code PH/Sk
   Naval Postgraduate School.
   Monterey, CA 93943-5117

4. Prof. Ching-Sang Chiu 1
   Oceanography Department, Code OC/Ci
   Naval Postgraduate School.
   Monterey, CA 93943-5122

5. CDR Mitchell Shipley 1
   Physics Department, Code PH/SM
   Naval Postgraduate School.
   Monterey, CA 93943-5117

6. Stephen Greineder 2
   Naval Undersea Warfare Center, Division Newport
   Code 2121, Bldg. 1320, Room 380
   Newport, RI 02841

7. Instituto de Pesquisas de Marinha 1
   Rua Ipiru, s/n$^{\underline{o}}$
   Ilha do Governador, Rio de Janeiro, RJ
   BRAZIL - CEP 21931-090

8. LT Arthur F. Bettega Correa 1
   IpqM - Rua Ipiru, s/n$^{\underline{o}}$
   Ilha do Governador, Rio de Janeiro, RJ
   BRAZIL CEP 21931-090